N85-25890

DIRECT TRANSIENT ANALYSIS OF A FUZE ASSEMBLY BY AXISYMMETRIC SOLID ELEMENTS

Chung C. Dai and Jackson C. S. Yang*
Advanced Technology & Research, Inc.
Burtonsville, MD 20866

John Titus
Harry Diamond Laboratory
Adelphi, MD 20783

ABSTRACT

A fuze assembly, which consists of three major parts, i.e., nose, collar and sleeve, was designed to survive severe transverse impact giving a maximum base acceleration of 20,000 G. Experiments showed that hoop failure occurred in the collar after the impact. They also showed that by bonding the collar to the nose, the collar was able to survive the same impact. To find out the effectiveness of the bonding quantitatively, axisymmetric solid elements TRAPAX and TRIAAX were used in modelling the fuze and direct transient analysis was performed. The dynamic stresses in selected elements on the bonded and unbonded collars were compared. The peak hoop stresses in the unbonded collar were found to be up to three times higher than those in the bonded collar. NASTRAN results successfully explained the observed hoop failure in the unbonded collar. In addition, static and eigen value runs were performed as checks on the models prior to the transient runs. Their results are compared with experiments. Comments on the use of the MPCAX cards, the existence and contributors of the calculated first several nearly identical natural frequencies, are also addressed.

INTRODUCTION

The M732 E2 Artillery Proximity Fuze comprises an aluminum fuze body which houses a safety and arming module, detonator bulkhead, and power supply aft of a center bulkead. Forward of the bulkhead is the fuze processor electronics and loop oscillator. The oscillator is housed in a 30% glass reinforced modified Polyphenylene Oxide (PPO) nose cone which is secured to the fuze body with a 30% glass reinforced PPO threaded retaining collar. See Figures 1 and 2.

When a projectile is fired from a gun, the fuze is subjected to side loads approaching 20,000 G's. In the laboratory, a machine was developed to simulate this loading. The fuze is secured to a rail guided steel fixture which is struck from the side by a steel weight. The impact is tailored to give a 20,000 G peak lateral acceleration with a 30 fps velocity change.

While fuzes at ambient temperature experienced no failures when subjected to the test, fuzes which were temperature conditioned at -40° F failed without exception. The major failure mode, named hoop failure, appeared to be hoop stress on the retaining collar causing a longitudinal crack from end to end. See Figure 3.

It was discovered that by solvent bonding the retaining collar to the nose cone during assembly. the low temperature failures could be avoided. Since the mechanism by which the solvent bond alleviated the problem was not well understood nor was the safety factor of the bond known. it was feared that future modifications to the fuze could not be evaluated with respect to the impact on the fuze joint integrity. Therefore. NASTRAN was used to model the forward section of the fuze in an attempt to better understand the behavior of the current design. and better predict the behavior of future designs.

NASTRAN MODEL

The given fuze forward section consists of three major parts. i.e., nose. collar and sleeve. As depicted in Figures 4a. 4b. and 4c. 105 TRAPAX and 9 TRIAAX elements were used to model this fuze and its interior electronic parts. These elements are inter-connected at 180 different rings or circles. Static and eigen value analyses were performed prior to the final transient runs. Numerical results from the static and eigen value runs were carefully examined and compared with the available experiment data. Constraint conditions and boundary conditons had been modified accordingly. We will discuss in more detail later.

TEST MODEL I

A cantilevered. hollow slender cylinder. as depicted in Figure 5a. was modelled by TRAPAX elements as a preliminary study. Stress analysis of this cylinder was performed. Axial pressure load or concentrated transverse tip loading was separately applied. Numerical results from these test cases provided basic understanding on TRAPAX's behavior and characteristics. Axial pressure loading condition was first considered. see Figure 5b. As expected. NASTRAN results showed that the cylinder's cross sections were displaced uniformly and axial stress was developed uniformly across each cross section.

Figure 5c shows the transverse tip loading condition. The cylinder was modelled by regular 8 x 2. 16 x 2. 32 x 1. 32 x 2. 64 x 1 meshes. Both the tip deflection and the bending stress at point A were checked for convergence with respect to mesh refinement. As noted in Table 1. with the same number of elements. 64 x 1 mesh gave better resuls than 32 x 2 mesh. Based on this observation, we used only one layer across the thickness of the real model.

TEST MODEL II

A cantilevered. hollow slender cylinder of different size (Figure 6) was used in the remaining preliminary studies. It was modelled also by TRAPAX elements but with 4 x 1 or 5 x 1 mesh. This model served for testing NASTRAN rigid formats 3. 9, and 12. simulating the prescribed base acceleration. and also for testing NASTRAN checkpoint and restart features.

Free vibration analysis was performed on the cantilevered hollow cylinder in Figure 6a. Different frequency ranges were specified requesting the extraction of natural frequencies and modes.

Given V = 30 ft/sec after the impact and the maximum acceleration of 20,000g, the duration of the impulse depends on the assumption of its shape. For a $\sin\omega t$ shaped impulse, the duration is about 70×10^{-6} sec. For a $\sin^2\omega t$ shaped impulse, the duration is about 90×10^{-6} sec. Impulses of both shapes were tested on Model II. However, only the $\sin^2\omega t$ shaped impulse was employed in the analysis of the real model because it simualtes the real impulse more closely.

Several schemes to input the prescribed base acceleration a(t) were also carefully examined. First, a nearly rigid layer with huge mass M was attached to the bottom of the original cylinder. Dynamic force F(t) = Ma(t) was then applied to this layer in several ways to achieve the desired prescribed base motion. The dynamic force can be directly applied to the COSINE term of the ring No. 2 in Figure 6b. It can also be applied, using POINTAX cards, at selected points in the bottom layer. As observed in the test runs, both approaches gave the same results. The "POINTAX" approach was taken on the real model.

The appropriate E/ρ ratio was determined to be of the order of 10^{20}. This specific ratio gave an uniform base acceleration as desired. In addtition, both CONEAX and TRAPAX elements were tested out as the base layer. The TRAPAX element was employed in the real model.

Modal transient analysis was performed on this test model. However, as noted from the eigen value analysis on the real model, there are a large number of natural modes in the low frequency range. Also, the impulse duration is so short that modes with extremely high frequencies are expected to participate in the dynamic response. Obviously, modal transient approach will not be accurate without using a large number of modes, which in turn will make it extremely time-consuming. Therefore, direct transient approach was taken for the analysis of real model.

STATIC ANALYSIS

Static analysis of both bonded and unbonded cases were performed as checks on the fuze model. The load condition considered was that of 100 lbs. transversely applied at node 9.

For this loading case, deflections at the load point and nodes 17, 21, are listed for different choices of harmonic terms. (See Table 2) Based on its convergence characteristics, AXIC = 3 was specified for the transient analysis. This means one constant and three harmonic functions were combined to describe the deformation field along the circumferential direction. Stress distribution in different parts were examined, and the MPCAX cards were modifid accordingly to achieve appropriate constraints between nose, collar and plate.

In order to calibrate the model, simple experiments were devised to perform static tests on the fuze nose cones. A force gage was used to apply a static load onto the tip of the fuze. The fuze was mounted in a rigid base and a dial indicator was used to record the fuze deflection at the point of the load. The test setup is shown in Figure 7.

Loads were applied near the tip of the fuze, incrementing the load from 20 lbs. to 140 lbs. and recording the deflection of each increment. This test was performed for bonded sample of the fuze. Comparison of NASTRAN and experiment results is in Table 3. Note that the noticeable differences may have been caused by the fact that the tip of the force gage made a slight indentation in the surface of the nose cone.

EIGEN VALUE ANALYSIS

Eigen value analysis were performed to further check the appropriateness of the NASTRAN model. MPCAX conditions between nose-collar-plate were repeatedly examined and modified. The final arrangement of these conditions is listed in Table 4. This specific arrangement induces only relatively low stress in the plate while maintaining stability of the model. It is worth mentioning that in the seventh field of the MPCAX Card, the HID number should take he form of (Integer ≥ 0) instead of (Integer > 0). Otherwise, undesirable rigid body modes may be present in the model.

Ten fundamental frequencies and modes were extracted for both bonded and unbonded cases. As listed in Table 5, the first 9 eigen values of both cases are exactly the same. Also from Table 5, the lowest four frequencies are very close together at 30 cps. It was identifed, very interestingly, that each harmonic contributed to one of them.

DIRECT TRANSIENT ANALYSIS

Transient responses from t = 0 sec to t = 270×10^{-6} sec, which was three times the impulse duration, were obtained for both bonded and unbonded cases. Solution convergence with respect to different time steps is listed in Table 6. $\Delta t = 2 \times 10^{-6}$ sec was chosen for the time increment in the analysis. The base displacement time history compared very well with the prescribed one. The dynamic stresses in the plane of impact in elements 104 and 105 were plotted and compared between both cases (see Figures 8-11).

Figures 8 and 10 show the hoop stress time histories of both cases. The peak hoop stress in unbonded collar is up to about three times higher than that in the bonded collar. This explains the hoop failure in the unbonded collar as was observed from experiments.

Figures 9 and 11 show the axial stress time histories of both cases. The peak axial stress in bonded collar is significantly higher than that in the unbonded collar.

CONCLUSION

The NASTRAN results presented in Figures 8 through 11 lead to the following conclusion:

By bonding the nose and the collar, the nose joint will take dynamic load mainly in the form of axial stress. The peak hoop stress experienced in the bonded collar will thusly be reduced by a factor of 4. Hence, the hoop failure was effectively avoided in the bonded collar.

TABLE 1. SOLUTION CONVERGENCE WITH RESPECT TO MESH REFINEMENT

MESH	ASPECT RATIO	TIP DEFLECTION	BENDING STRESS AT POINT A
8 x 2	7.5	0.001832	---
16 x 2	3.75	0.003029	798
32 x 1	0.94	0.003568	2151
32 x 2	1.875	0.003631	2085
64 x 1	0.47	0.003775	2314
ANALYTICAL	----	0.003918	2292

TABLE 2. CONVERGENCE OF LATERAL DEFLECTION
WITH RESPECT TO THE NUMBER OF HARMONICS (BONDED COLLAR)

NO. OF HARMONICS	LATERAL DEFLECTION		
	NODE 9	NODE 17	NODE 21
3	-0.00676	-0.00467	-0.00375
4	-0.00737	-0.00467	-0.00375
7	-0.00767	-0.00467	-0.00375

TABLE 3. COMPARISON OF STATIC RESULTS
(TRANSVERSE LOAD AT 0.27" FROM NOSE TIP)

CASE	EXPERIMENT	NASTRAN
BONDED	-0.014	-0.00676
UNBONDED	-0.020	-0.00821

TABLE 4. CONSTRAINT CONDITIONS ON HARMONICS BETWEEN NOSE, COLLAR AND PLATE

CONSTRAINED RING PAIRS		BONDED			UNBONDED		
		r	θ	z	r	θ	z
35	235	0-3	0-3	0-3	0-3	0-3	0-3
37	237	0-3	0-3	0-3	0-3	0-3	0-3
40	240	0-3	0-3	0-3	0-3	0-3	0-3
43	243	0-3	0-3	0-3	0-3	0-3	0-3
46	246	0-3	0-3	0-3	0-3	0-3	0-3
49	249	0-3	0-3	0-3	0-3	0-3	0-3
52	252	0-3	0-3	0-3	0-3	0-3	0-3
55	255	0-3	0-3	0-3	0-3	0-3	0-3
58	258	0-3	0-3	0-3	0-3	---	0-3
60	260	0-3	0-3	0-3	0-3	---	0-3
63	263	0-3	0-3	0-3	0-3	---	0-3
64	364	---	---	0	---	---	0
65	365	0,1	---	0,1	0,1	---	0,1
70	370	---	---	0,1	---	---	0,1

EIGEN VALUE ANALYSIS BONDED NOSECONE

MODE NO.	EXTRACTION ORDER	EIGENVALUE	REAL EIGENVALUES RADIAN FREQUENCY	CYCLIC FREQUENCY
1	6	3.611820E+04	1.900479E+02	3.024706E+01
2	5	3.626425E+04	1.904317E+02	3.030815E+01
3	7	3.642207E+04	1.908457E+02	3.037402E+01
4	4	3.648683E+04	1.910153E+02	3.040102E+01
5	2	9.198356E+04	3.032878E+02	4.826976E+01
6	1	1.029579E+05	3.208706E+02	5.106813E+01
7	3	1.211922E+05	3.481267E+02	5.540608E+01
8	8	2.205529E+05	4.696306E+02	7.474403E+01
9	10	3.234188E+05	5.686992E+02	9.051129E+01
10	9	3.374114E+05	5.808713E+02	9.244855E+01

EIGEN VALUE ANALYSIS UNBONDED NOSECONE

MODE NO.	EXTRACTION ORDER	EIGENVALUE	REAL EIGENVALUES RADIAN FREQUENCY	CYCLIC FREQUENCY
1	6	3.611820E+04	1.900479E+02	3.024706E+01
2	5	3.626425E+04	1.904317E+02	3.030815E+01
3	7	3.642207E+04	1.908457E+02	3.037402E+01
4	4	3.648683E+04	1.910153E+02	3.040102E+01
5	2	9.198356E+04	3.032878E+02	4.826976E+01
6	1	1.029579E+05	3.208706E+02	5.106813E+01
7	3	1.211922E+05	3.481267E+02	5.540608E+01
8	9	2.205529E+05	4.696306E+02	7.474403E+01
9	10	3.234188E+05	5.686992E+02	9.051129E+01
10	9	3.246078E+05	5.697437E+02	9.067752E+01

TABLE 5. FIRST TEN NATURAL FREQUENCIES OF FUZE EXTRACTED FROM NASTRAN

TABLE 6. CONVERGENCE OF TRANSIENT SOLUTIONS WITH RESPECT TO TIME STEP SIZE

BASE MOTION	$\Delta t = 4\mu$ sec	$\Delta t = 2\mu$ sec	$\Delta t = 1\mu$ sec	$\Delta t = 0.5\mu$ sec
Acceleration At:				
$t = 8\mu$ sec	6.7×10^5	6.08×10^5	5.98×10^5	5.92×10^5
$t = 10\mu$ sec	---	9.22×10^5	9.13×10^5	9.09×10^5
Displacement At:				
$t = 8\mu$ sec	5.53×10^{-6}	3.77×10^{-6}	3.47×10^{-6}	3.4×10^{-6}
$t = 10\mu$ sec	---	8.63×10^{-6}	8.17×10^{-6}	8.06×10^{-6}

FIGURE 1
ADVANCED PROX FUZE CONCEPT

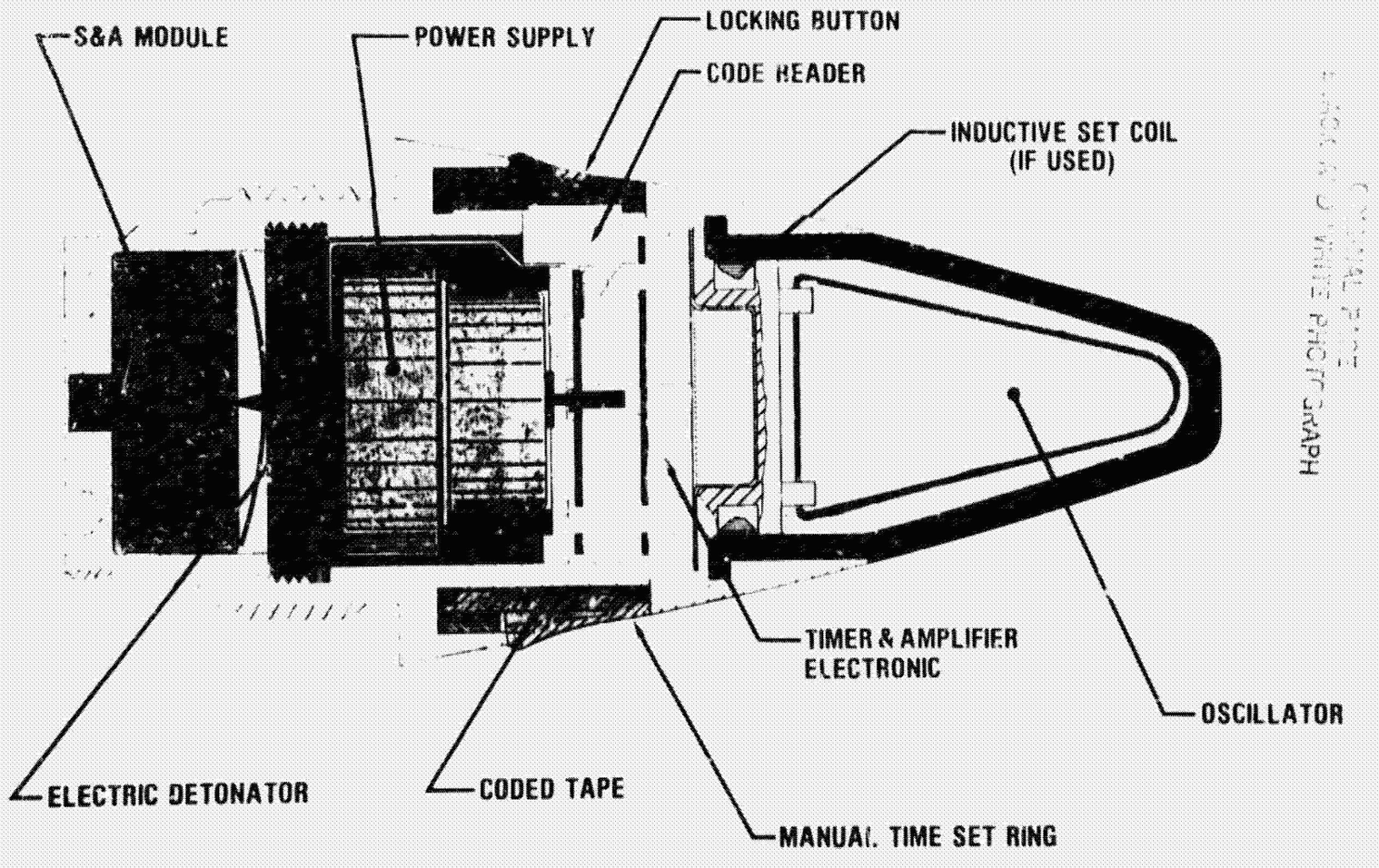

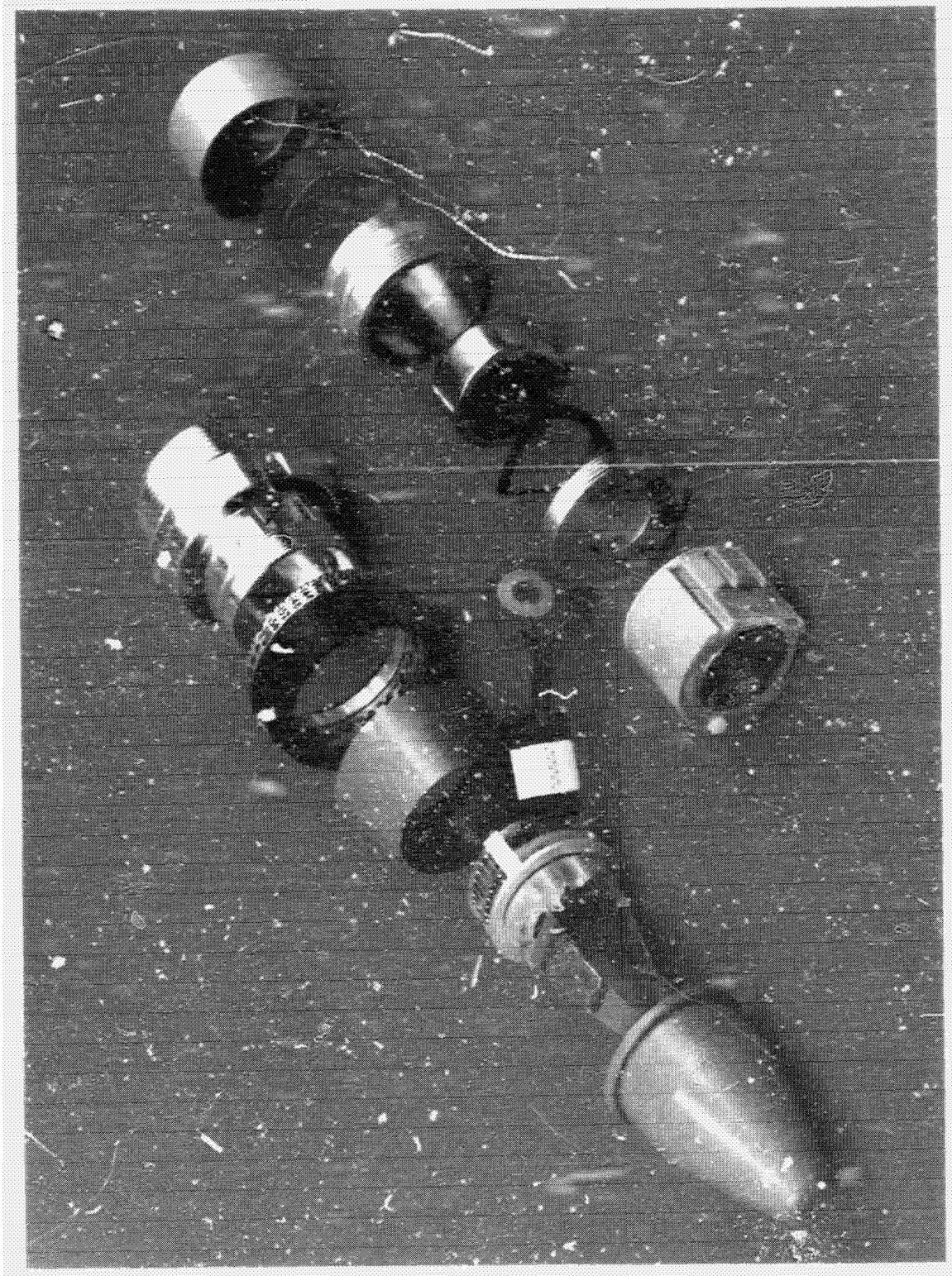

FIGURE 2

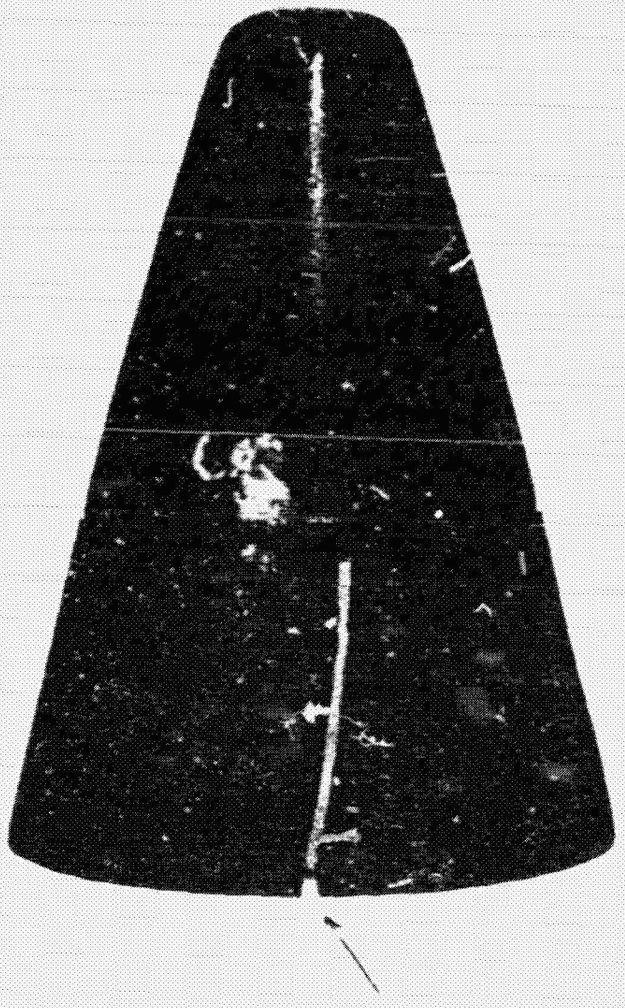

Figure 3 - Crack in the Retaining Collar

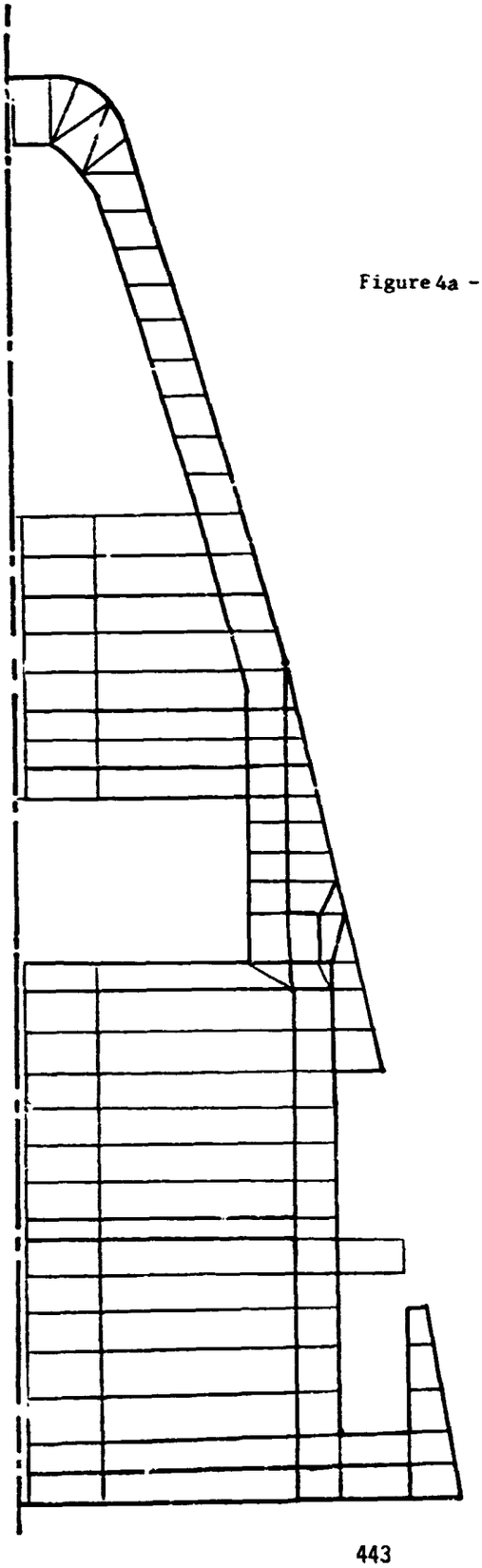

Figure 4a - Finite Element Mesh
Of The Fuze Assembly

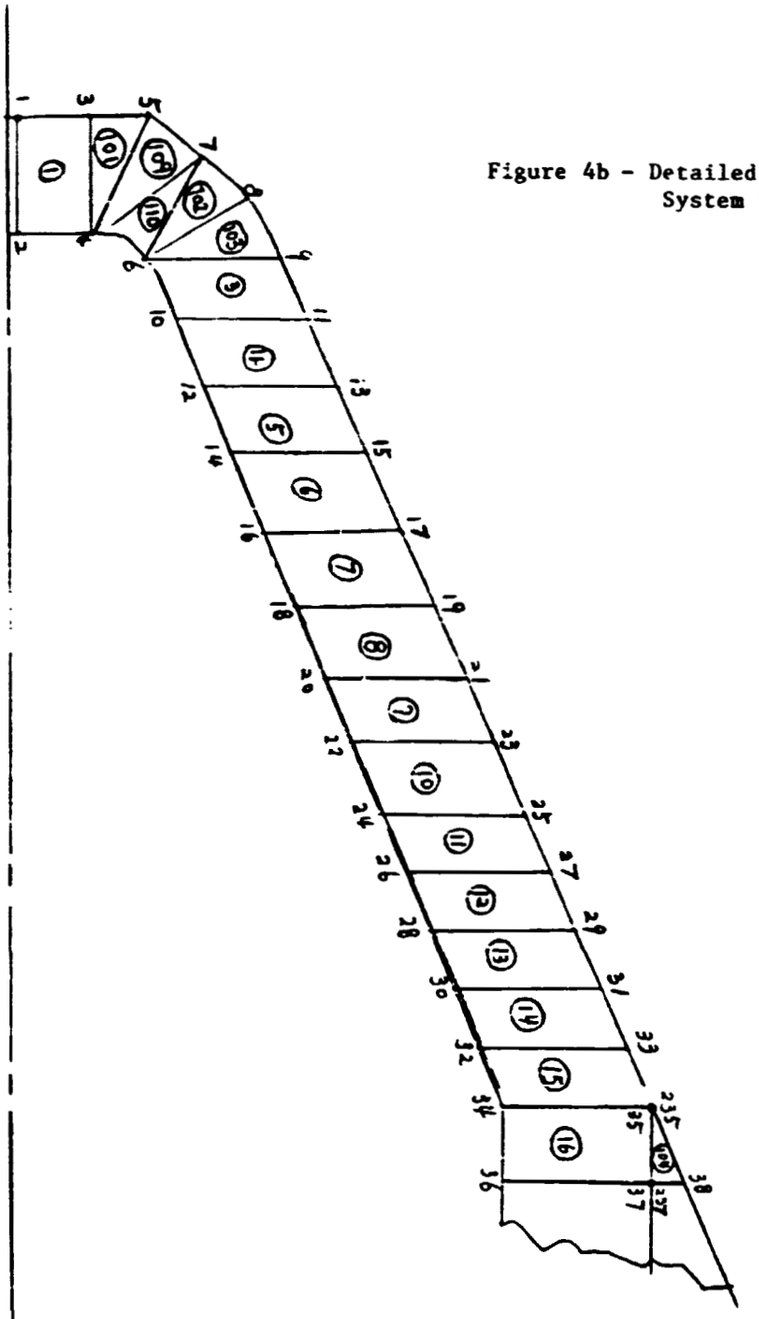

Figure 4b - Detailed Mesh Numbering System (Ncse)

ORIGINAL PAGE IS
OF POOR QUALITY

Figure 4c - Detailed Mesh Numbering System (Collar, Sleeve and Plate)

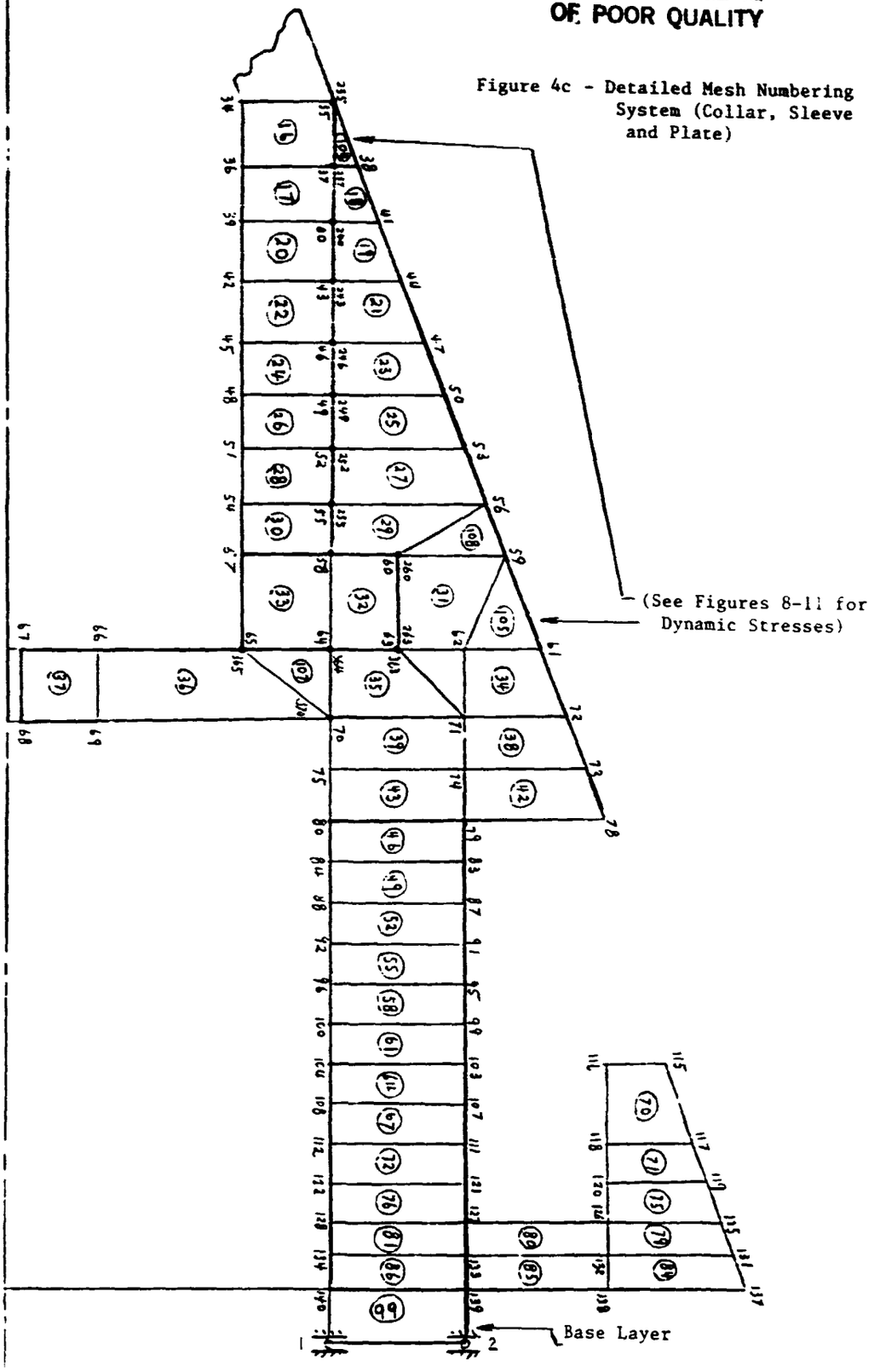

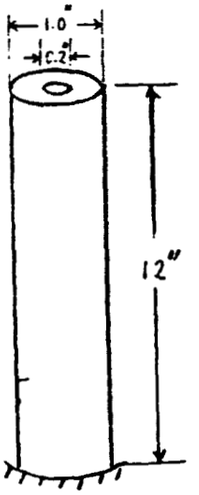

Figure 5a - Test Model I

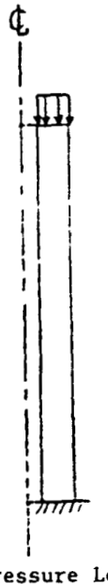

Figure 5b - Axial Pressure Loading Condition

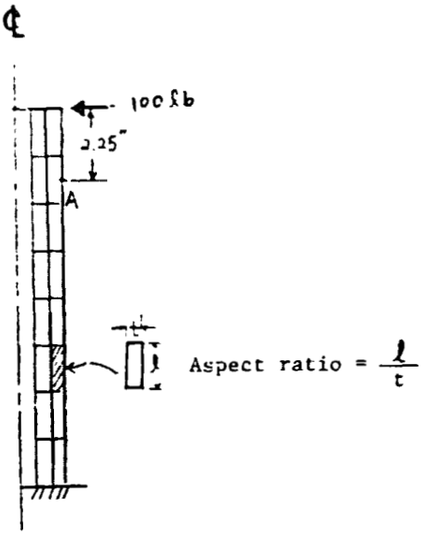

Figure 5c - Transverse Tip Loading Condition (8 x 2 Mesh)

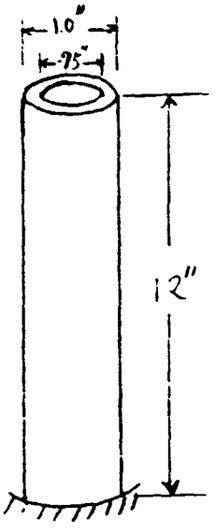

Figure 6 - Test Model II

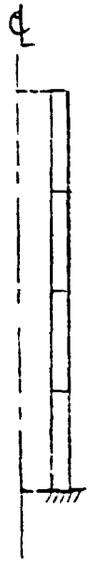

Figure6a FEM Model For
Free Vibration Analysis
(4 x 1 Mesh)

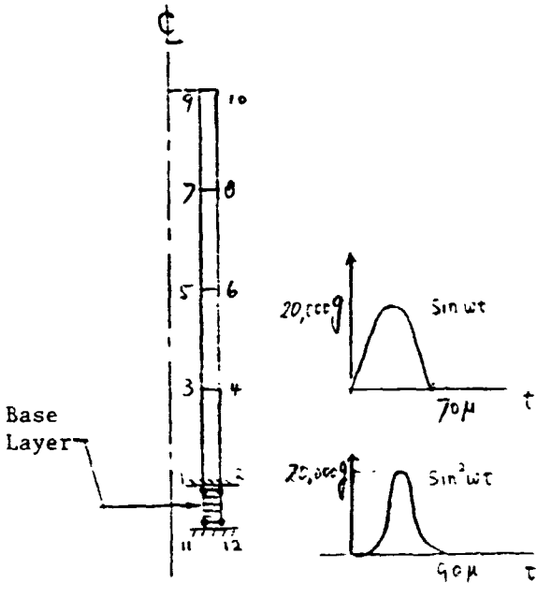

Figure 6b - FEM Model And Base
Excitations Transient Analysis
(5 x 1 Mesh)

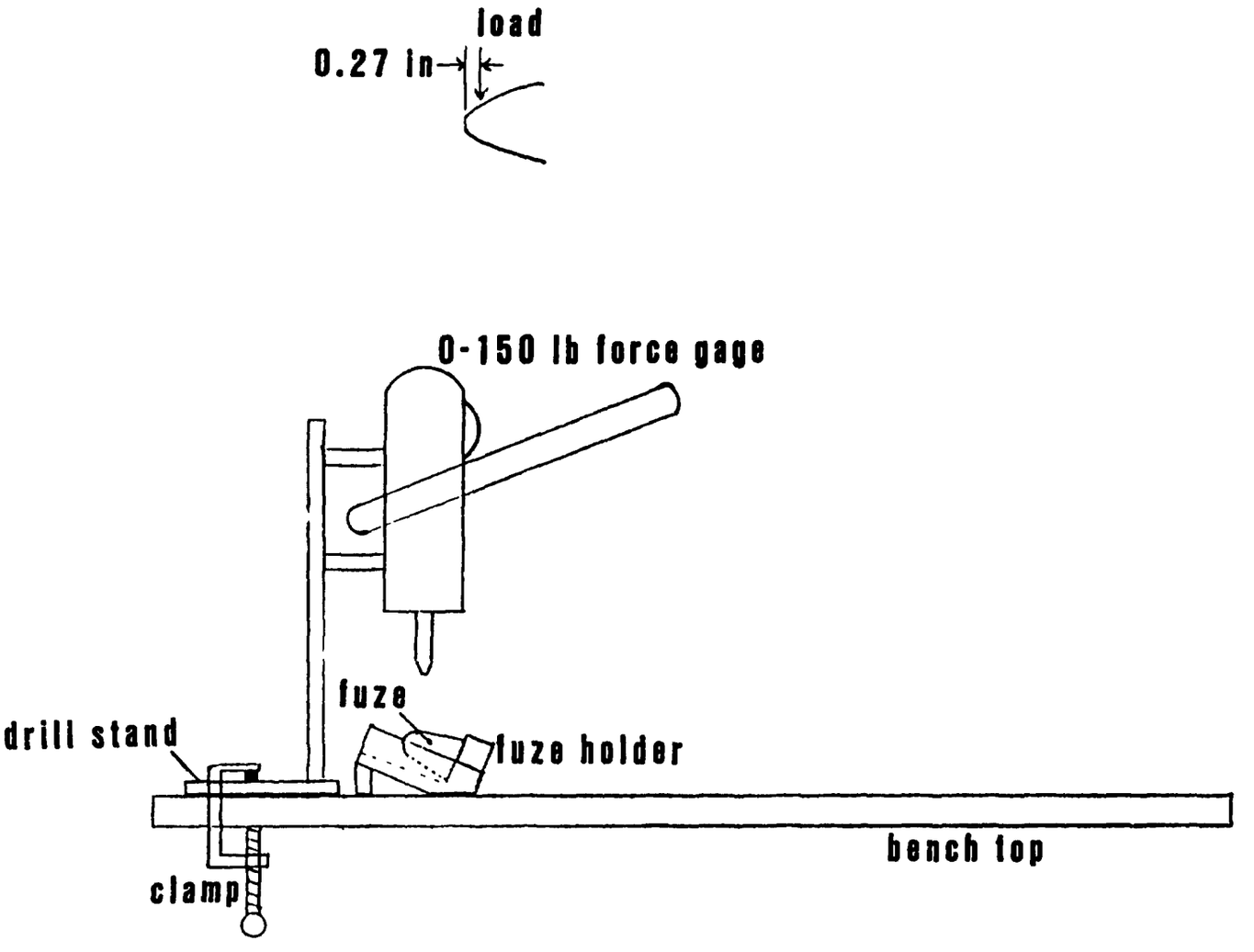

Figure 7. Test equipment setup

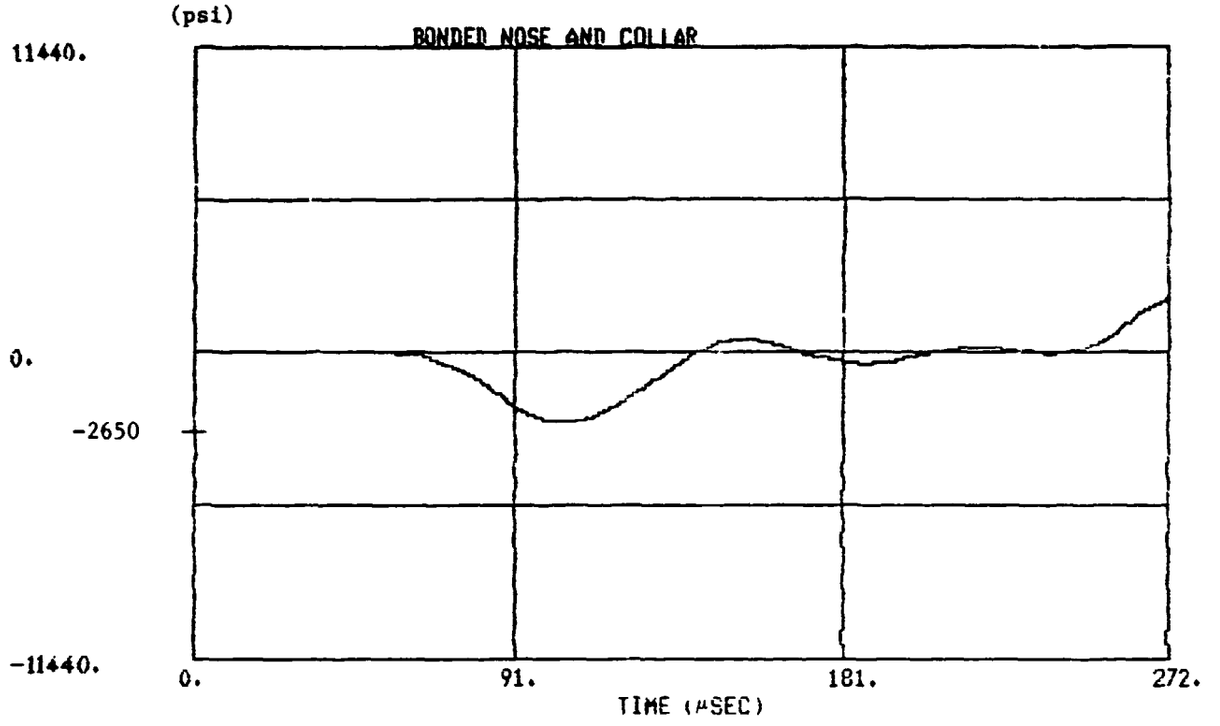

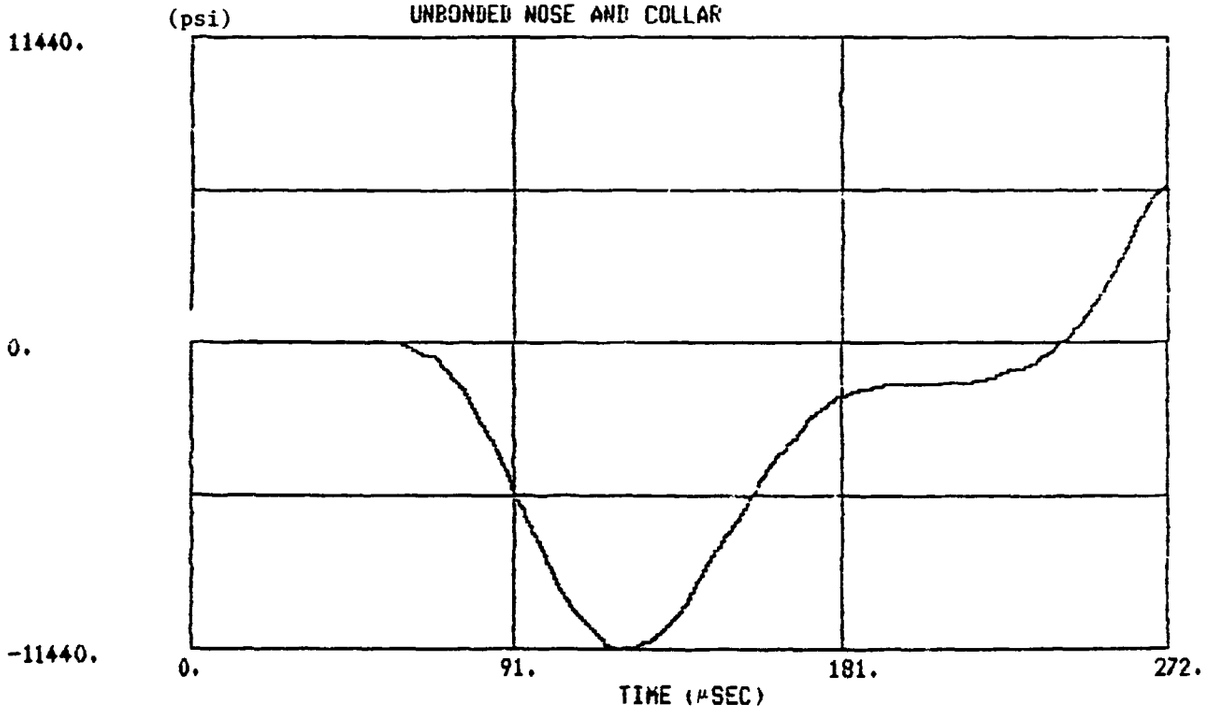

Figure 8 - Dynamic Hoop Stresses (Element 104)

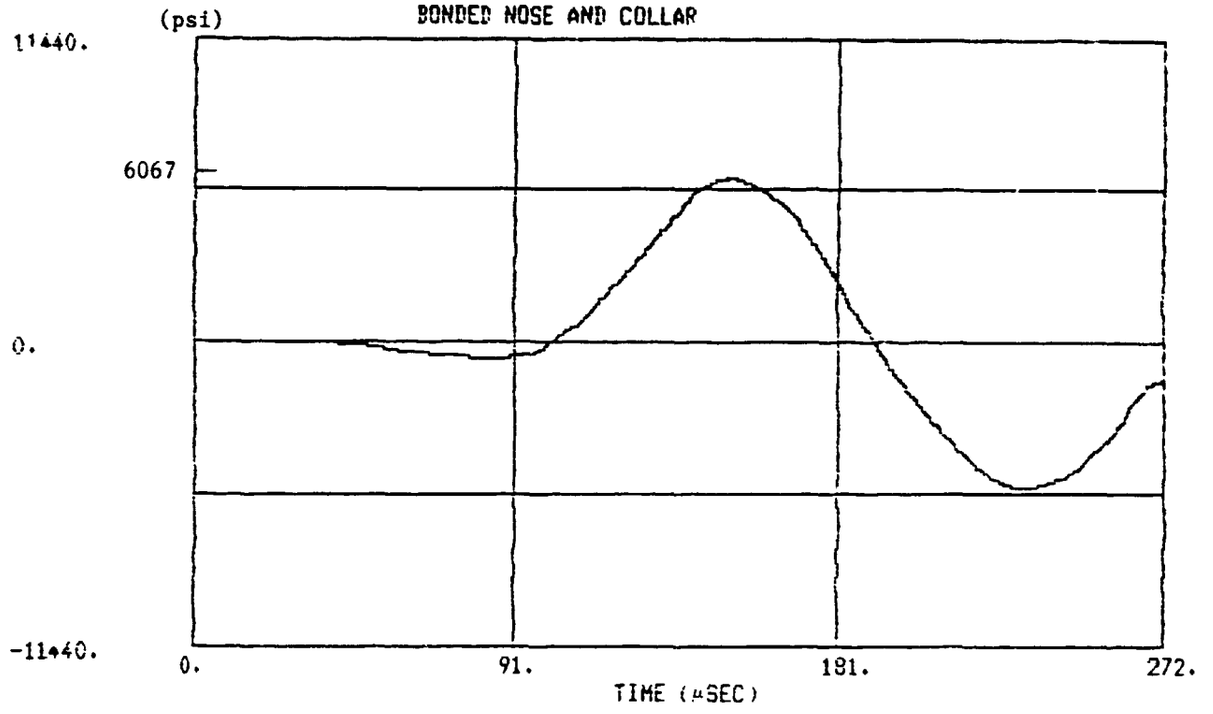

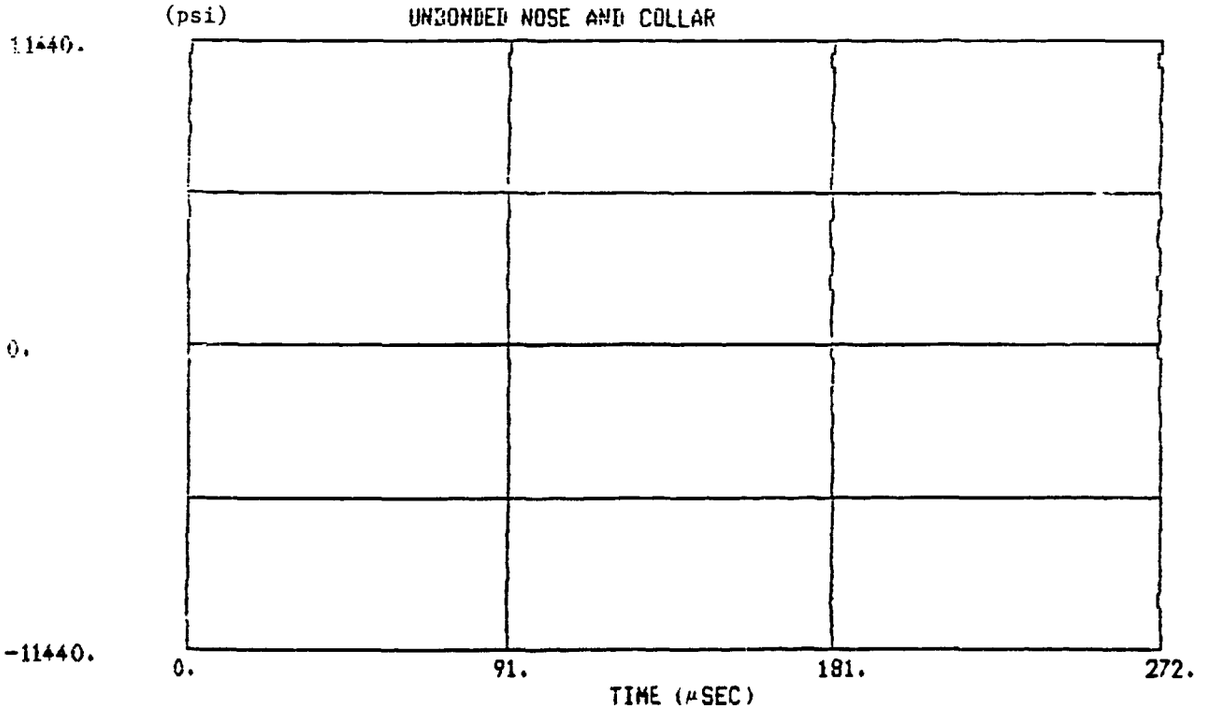

Figure 9 - Dynamic Axial Stresses (Element 104)

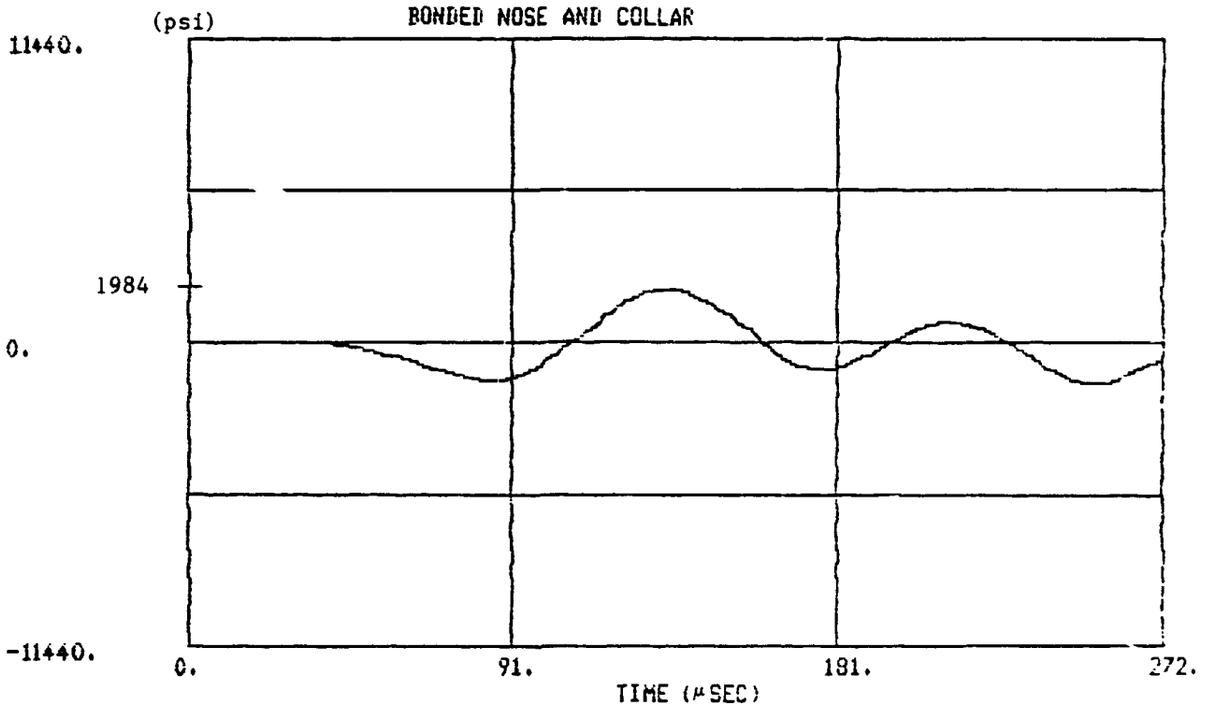

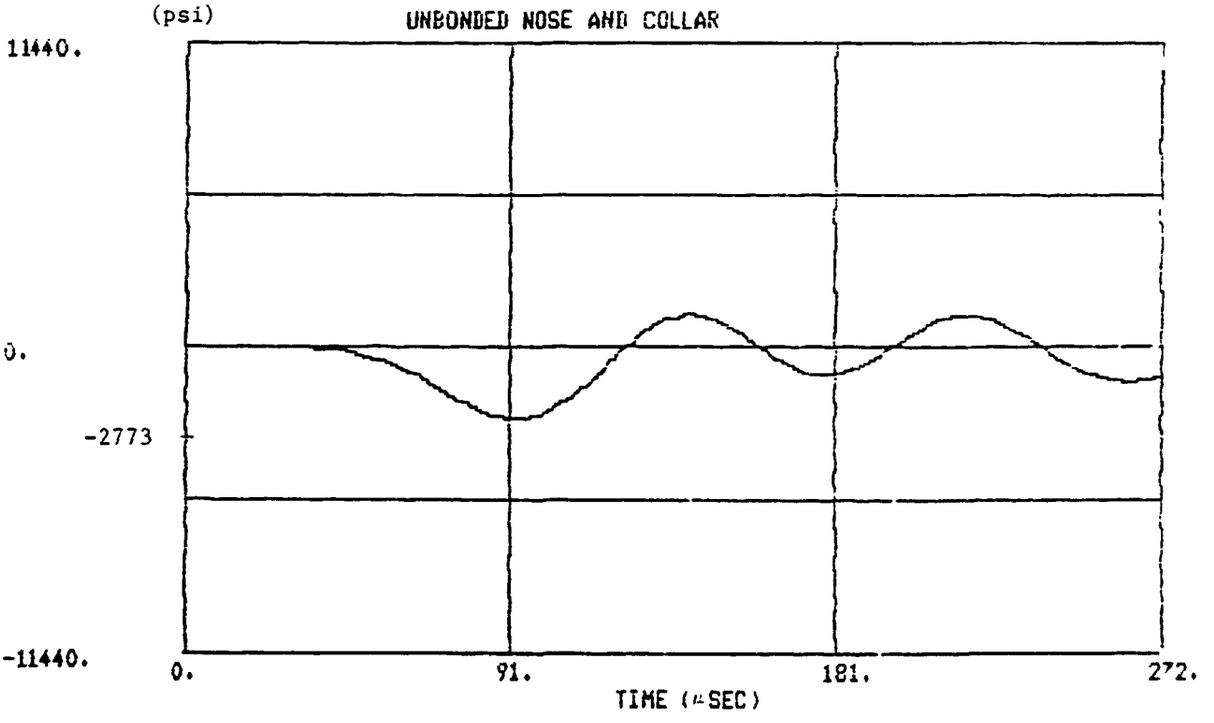

Figure 10 - Dynamic Hoop Stresses (Element 105)

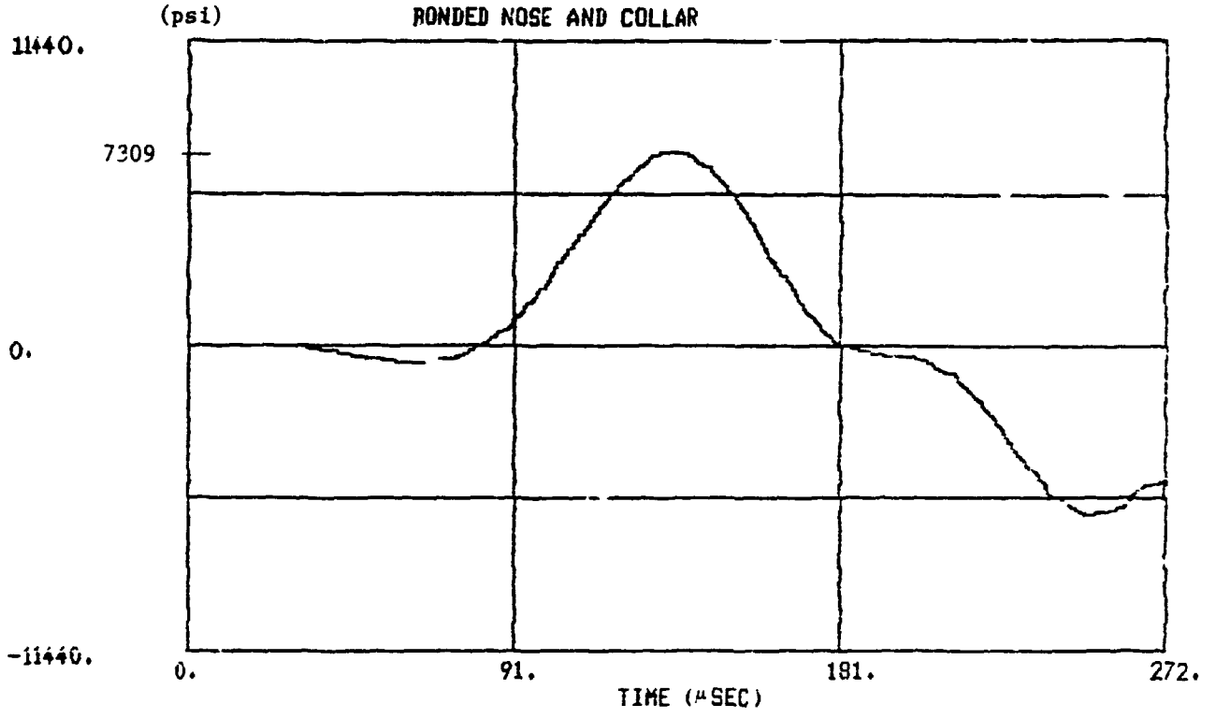

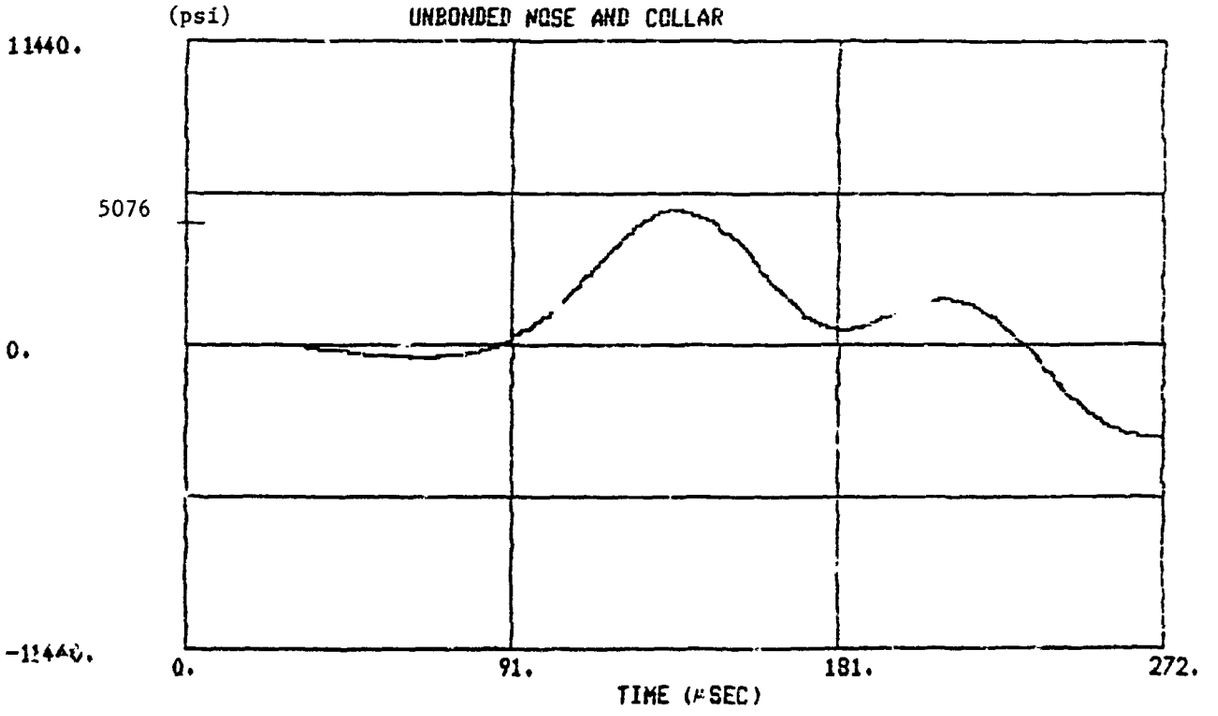

Figure 11 - Dynamic Axial Stresses (Element 105)